Journal of ELECTRONIC MATERIALS, Vol. 48, No. 11, 2019
https://doi.org/10.1007/s11664-019-07563-2

Effect of Tin Element on the Structural, Optical and Humidity Sensing Properties of Cerium Oxide Nanoparticles

S. VIGNESELVAN,[1,5] V. MANIKANDAN,[2] IULIAN PETRILA,[3] A. VANITHA,[1,6] and J. CHANDRASEKARAN[4]

1.—Department of Physics, Government College of Technology, Coimbatore 641 013, India. 2.—Department of Physics, Kongunadu Arts and Science College, Coimbatore 641 029, India. 3.—Faculty of Automatic Control and Computer Engineering, Gheorghe Asachi Technical University of Iasi, Str. Dimitrie Mangeron, Nr. 27, 700050 Iasi, Romania. 4.—Department of Physics, Sri Ramakrishna Mission Vidyalaya College of Arts and Science, Coimbatore 641 020, India. 5.—e-mail: skselvan555@gmail.com. 6.—e-mail: avanitha1973@gmail.com

In this work, pristine and tin substituted cerium oxide nanoparticles (NPs) namely $Ce_{1-x}Sn_xO_2$, x = 0.0, 0.2, 0.4, 0.6, were prepared by a simple microwave synthesis method for humidity sensing studies. Different characterization methods such as scanning electron microscopy, transmission electron microscopy and energy-dispersive x-ray spectroscopy analysis demonstrated the formation of spherical NPs with an approximate crystalline size of 5–10 nm, desirable chemical composition and presence of oxygen defects. Also, optical measurements results demonstrated the increase of the band gap energy in tin substituted NPs due to formation of intermediate energy levels as a result of tin substitution. Furthermore, humidity sensing studies showed a high response of the fabricated sensors to humidity as a result of very small particle sizes along with the presence of tin in cerium oxide NPs. Finally, the fabricated humidity sensors showed a very good reproducibility of 95%. The results of this study confirm the possibility of realization of highly sensitive humidity sensors based on tin substituted cerium oxide NPs for application in real environments.

Key words: Tin substituted cerium oxides, optical properties, structural properties, humidity sensor

INTRODUCTION

Cerium oxide (CeO_2) is a rare earth semiconducting metal oxide, which due to having a wide band gap energy, a large exciton binding energy and good physical and chemical properties, has been used in different applications such as catalysts, sensors, solid oxide fuel cells, sun screen cosmetics and antibacterial activity applications.[1] Furthermore, it has a unique electrochemical activity and is among the dominant materials used in different environmental applications.[2] Different synthesis methods such as the aqueous route has been used to synthesize the modified materials with controlled particle sizes.[3]

In CeO_2 lattice each Ce atom is surrounded by eight oxygen atoms and therefore, it has cubic-fluorite symmetry.[4] Regarding humidity sensing studies, in recent years, great efforts have been made to develop highly sensitive sensors, and it has been found that for practical usages the sensors should have a high and fast response, good reproducibility, wide range of relative humidity detection, chemical stability and as well as low prices.[5] In general, different semiconducting metal oxides have been widely used for detection of humidity and toxic gases due to good mobility of charge carriers, high stability and possibly of tuning of different properties through decrease of particle size and well as chemical modification.[6,7]

(Received February 13, 2019; accepted August 14, 2019; published online August 29, 2019)

Despite having good potential for realization of humidity sensors, less attention has been paid to humidity sensing properties of CeO_2.[8] To enhance the humidity sensing properties of CeO_2, tin element can be used as a substituted element. In fact, tin has a d^{10} electronic configuration which can lead to a better sensing performance.[9] In most cases, the substituted element changes the particle size of CeO_2 and this can greatly affect the sensing response. Furthermore, the substituted elements can significantly change the crystalline size,[10] shape[11] and crystallinity [12] of the host material.

Narsimha et al.[13] fabricated a polyaniline/CeO_2 composites humidity sensor with a linear response to humidity. Also, Pradip et al.[14] reported a humidity sensor based on CeO_2 with a fast response time, excellent reproducibility, long term stability and a wide range of humidity detection. The humidity sensors are essential for humidity monitoring in environments. Even though, there are different kinds of humidity sensors, their sensitivity is not often satisfying.

According to the above explanations, tin substituted CeO_2 NPs can be a good material for realization of robust and reliable humidity sensors. In this paper, the pristine and tin substituted CeO_2 NPs ($Ce_{1-x}Sn_xO_2$, x = 0.0, 0.2, 0.4, 0.6) were prepared by a microwave oven synthesis method. This method has advantages such as short preparation time, possibility of particle size control and also low price. The crystalline size of prepared NPs was in the range of 5–10 nm which led to a high surface area that is beneficial for sensing studies. Structural and optical properties of the synthesized NPs were studied. Also, humidity sensing tests were performed under three different environments, namely ideal, real and corrosive environments. The prepared NPs shows superior sensitivity at ideal and real environments. The main novelty of this work is good sensing performance of tin substituted CeO_2 at room temperature which was higher than that of pristine CeO_2 NPs.

EXPERIMENTAL METHOD

Synthesis of Tin Substituted CeO_2 NPs

The tin substituted CeO_2 NPs were synthesized using a microwave oven synthesis method. The starting materials, namely tin chloride and cerium chloride in analytical grade, were purchased from chemical companies. The goal was the synthesis of $Ce_{1-x}Sn_xO_2$, x = 0.0, 0.2, 0.4, 0.6 NPs. Accordingly, the desirable ratios of the chemicals were separately dissolved in 50 mL of de-ionized water and continuously stirred for 12 h. As a result a transparent solution with yellow colour was obtained. A sodium hydroxide solution was prepared and was used as precipitate agent. This solution was added to the yellow-coloured solution and upon reaching the solution pH to 11, the solution changed to a paste gel form. The above paste was washed for several times by de-ionized water. After washing, it was put into a bowl and then it was inserted into a microwave oven. In the microwave oven, the paste was dried at the interval of 30 ms over the day. After the process, the dried content was milled and became converted to the fine powders. Finally, the powders were annealed in a muffle furnace at 450°C for 5 h.

Characterization

Crystalline phases of pristine and tin substituted CeO_2 NPs were obtained by x-ray diffraction (XRD, Rigaku). Powder morphology and elemental analysis were studied using scanning electron microscopy (SEM) and transmission electron microscopy (TEM). Chemical composition was studied by energy-dispersive x-ray spectroscopy (EDX) analysis. Vibrational spectra were acquired by a Fourier transform infrared spectroscopy (FTIR) over the range of 400–4000 cm^{-1}. Optical absorption spectra were obtained using a UV–Vis spectrometer.

Humidity Sensing Tests

The pristine and tin substituted CeO_2 NPs were pressed into pellets using a hydraulic pelletizer. Then the copper electrodes were applied on the two faces of a pellet with help of silver paste and humidity sensors were prepared. Humidity tests were performed through an Agilent E 4980A LCR meter at room temperature, over the range of 0–100%RH. With help of de-ionized water and sodium chloride solution, humidification was prepared. Humidification was sprayed in the form of water vapour which cancels out the condensation on the surface of the material. The test was carried out at different environments, namely ideal, real and corrosive environments. Humidification values are described by relative humidity (%RH).

RESULT AND DISCUSSIONS

XRD Analysis

Figure 1 shows the XRD patterns of pristine tin substituted CeO_2 NPs. The diffraction peaks correspond to (111), (200), (311), (400) and (331) crystalline planes of SnO_2 which matched with standard JCPDS Card No-34-0394.[15] No purity such as tin hydroxide was detected, which demonstrate the highly purity of the starting materials as well as a good synthesis method of employed. Upon tin substitution, the diffraction angles (2θ) were shifted to the higher angles due to difference between the ionic radii of cerium (0.114 nm) and tin (0.071 nm).[16] Tin element causes lattice distortion in the Ce crystal lattice, which led to shift of diffraction patterns. Particle sizes were decreased with increasing of the tin content. Furthermore, it has been reported that due to tin substitution, the amounts of the oxygen vacancies increased.[17] The particle size was calculated from the (111) peak of

CeO_2 which had the highest intensity. The well-known Scherrer formula was used to calculate the particle size;

$$D = \frac{k\lambda}{\beta \cos\theta}. \quad (1)$$

Here, D is the crystalline size, λ is the wavelength of x-ray (1.5409 Å), β is the full width at half maximum, θ is the Bragg angle in radian and k is a shape constant. The crystalline sizes were in the range 5–10 nm. XRD parameters are listed in Table I.

Surface Morphology and Elemental Analysis

The morphology of pristine and tin substituted CeO_2 NPs was obtained using SEM and is shown in Fig. 2a, b, c and d). The pristine CeO_2 NPs have a spherical shape and the observed spherical shape was slightly deformed due to the addition of tin. In fact, as a result of tin addition, the NPs were shrunken. In the meantime, agglomeration was increased due to the change of particle size. Figure 2e and f depicts the EDX spectrum of pristine and tin substituted CeO_2 NPs. The expected elements, namely, oxygen (O), cerium (Ce) and tin (Sn) were observed. Also, based on the EDAX result, the variation of the tin content led to increase of the oxygen defects due to the decrease of the particle sizes or deformation of the NPs.[18]

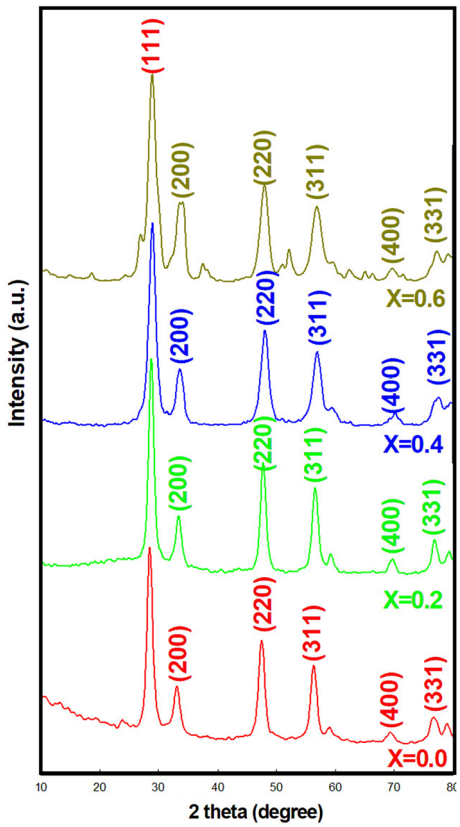

Fig. 1. XRD patterns of pristine and tin substituted CeO_2 NPs.

TEM Analysis

Figure 3a, b, c and d shows the TEM images of pristine and tin substituted CeO_2 NPs, respectively. The size of prepared NPs is in the range of 3–13 nm and the resultant particles have spherical shapes. Also, the crystallization of CeO_2 NPs is enhanced by tin addition. Most of the grains are homogeneous and uniform agglomeration has occurred between the particles. It has been reported that the agglomeration increases with decreases in the particle size due to high surface energy.[19] The measured particle sizes from TEM are in good accordance with the crystalline sizes calculated from XRD patterns (Table II).

FT-IR Study

The FT-IR spectra of pristine and tin substituted CeO_2 NPs are shown in Fig. 4a, b, c and d, respectively. The pristine CeO_2 NPs have few vibrations peaks and as a result of tin substitution, number of vibrations was increased due to the lattice distortion. The peak located at 3000–3750 cm^{-1} can be assigned to O–H stretching because of water and Ce–OH.[1] The peak located at 2923 cm^{-1} can be attributed to the C–H bonds of organic compounds.[20] The absorption peak located at 1400–2360 cm^{-1} is due to CO_2.[21] The peak located at 1620–1633 cm^{-1} can be assigned to the bending of H–O–H.[22] The peak at 1032–1340 cm^{-1} is due to Ce–O–Ce vibration.[21] The peaks around 400–434 cm^{-1} are due to Ce–O bonds.[12] Based on the FT-IR spectra, the presence of tin in the CeO_2 lattice is confirmed. Overall, the peak shift was found due to addition of tin content.

Table I. XRD and sensitivity parameters

Materials $Ce_{1-x}Sn_xO_2$	Particle size (nm)	Ideal environment sensitivity (%)	Real environment sensitivity (%)	Corrosive environment sensitivity (%)	Band gap energy (eV)
CeO_2 (x = 0.0)	10.98	64.47	62.21	45.85	2.63
Sn-CeO_2 (x = 0.2)	8.48	65.50	60.20	43.68	2.69
Sn-CeO_2 (x = 0.4)	6.45	72.66	68.37	43.98	2.82
Sn-CeO_2 (x = 0.6)	5.91	82.99	78.67	54.08	2.86

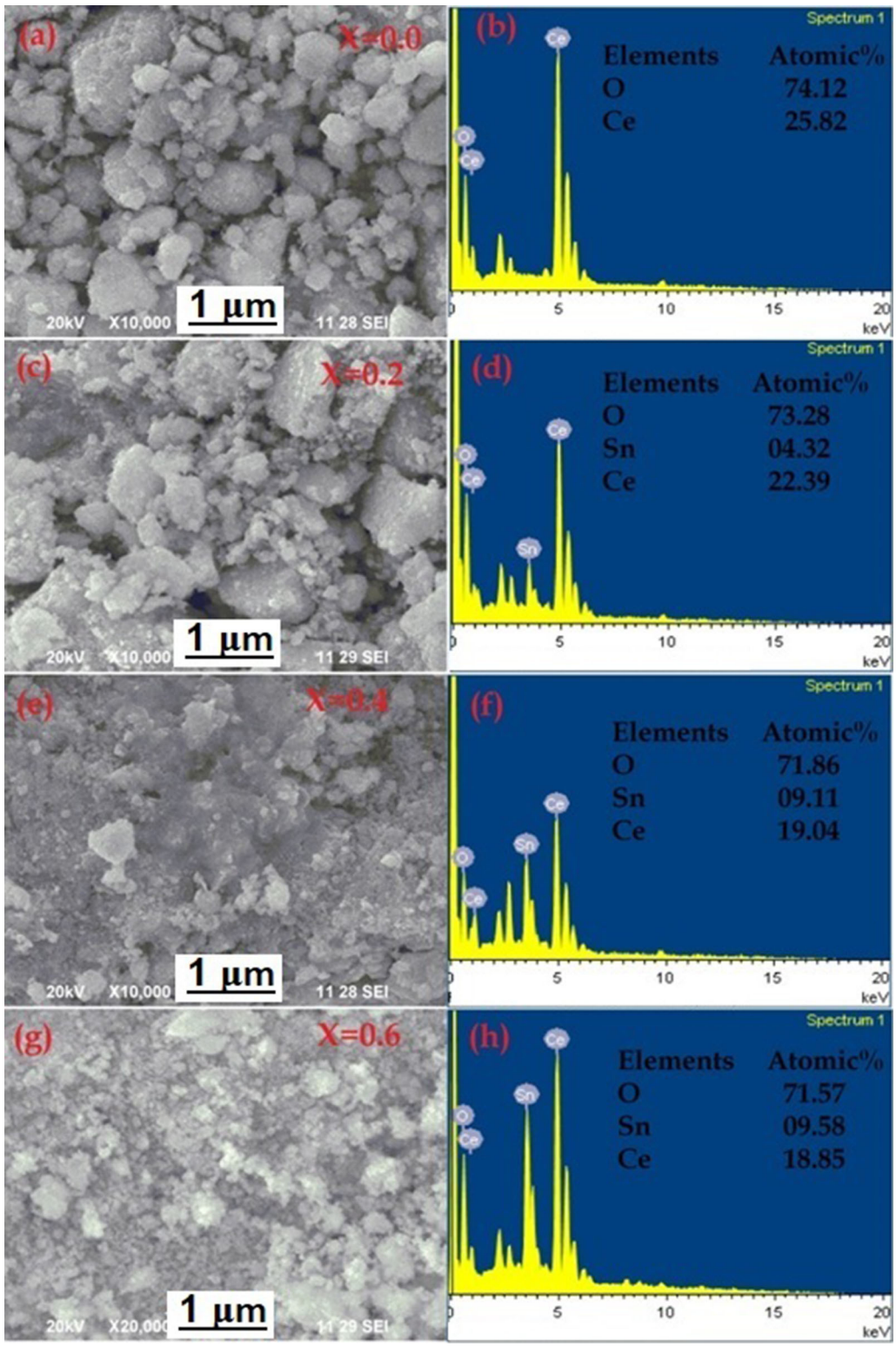

Fig. 2. SEM images and EDX spectrum (a–b) of pristine, (c–h) tin substituted CeO_2 NPs.

Optical Properties

The optical absorption of spectra of pristine and tin substituted CeO_2 NPs are shown in Fig. 5. The cut-off wavelength of prepared NPs was found to be below ~350 nm and no peaks related to the impurities were observed. Each absorption spectrum was blocked between 250 nm and 350 nm which allows

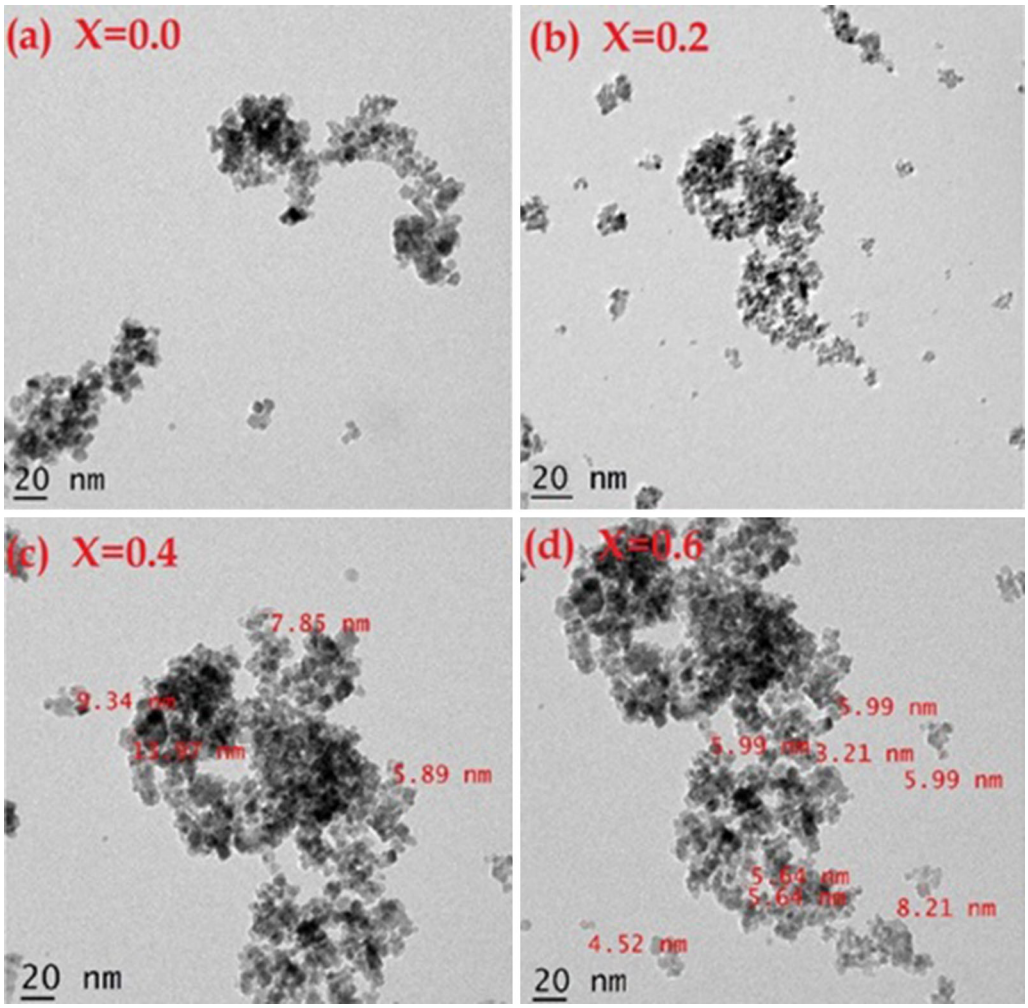

Fig. 3. (a) TEM image of pristine and (b–d) tin substituted CeO_2 NPs.

Table II. Comparison between reported humidity sensor and tin substituted cerium oxide sensor

S. no.	Materials	Sensitivity (%)	References
1	Silver nanoparticles	57	Ref. 30
2	ZnO/SnO_2 nanorod	75	Ref. 31
3	Graphene oxide	46	Ref. 32
4	$ZnTiO_3$	50	Ref. 33
5	ZnO	22	Ref. 34
6	AgNPs	40	Ref. 35
7	Sn-CeO_2	83	Present work

the NPs to be used as blocker. Additionally, each absorption spectrum showed a slight shift due to presence of tin element. The band gap energy was obtained from the absorption co-efficients and photon energy by the following equation[23];

$$E_g = h\nu - (\alpha h\nu)^{1/n}. \quad (2)$$

Here, α is the absorbance, h is the Planck's constant, ν is the frequency and E_g is the band gap energy. As shown in Fig. 6, the band gap values were increased from 2.63 eV to 2.86 eV, upon tin addition, which was due to the formation of the new level of energy intermediate.[24] The energy intermediate is associated with preparation method, shape, average particle size, chemical composition and structural disorder.

Humidity Sensing Properties

Figure 7 (a-f) depicts the humidity sensing response of pristine CeO_2 sensor. Upon exposure

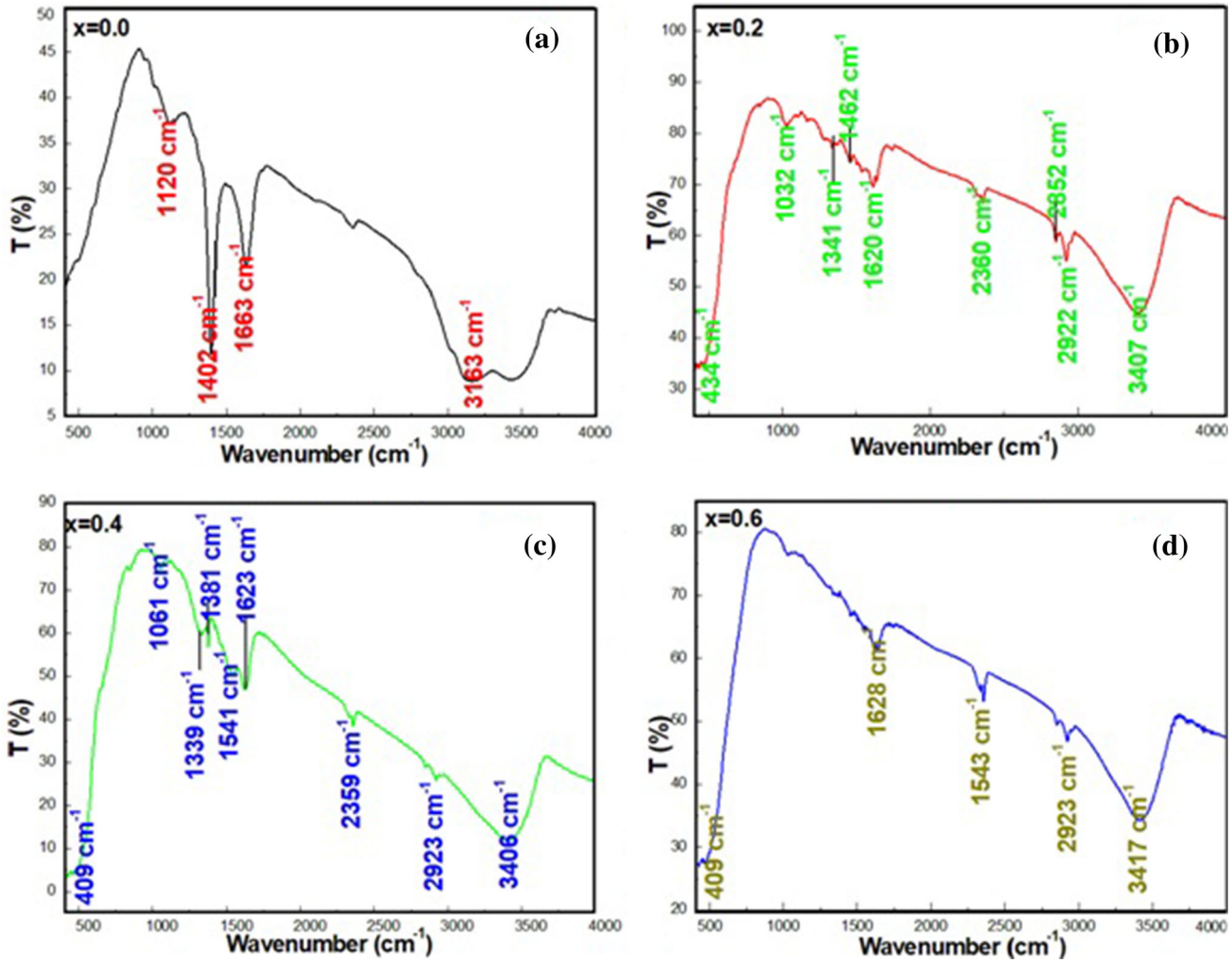

Fig. 4. (a) FTIR spectrum of pristine and (b–d) tin substituted CeO_2 NPs.

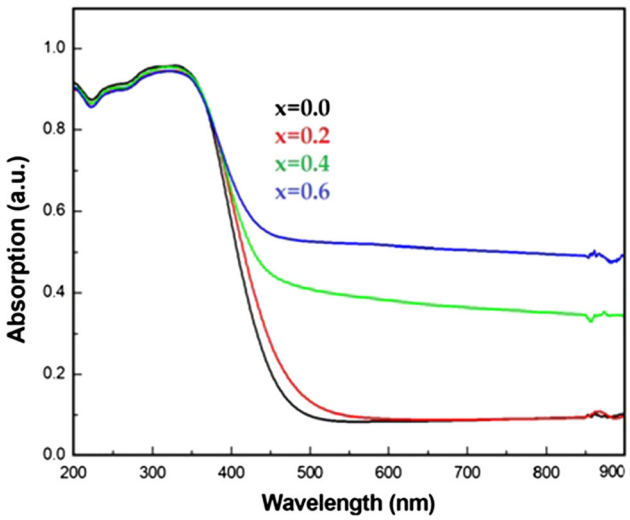

Fig. 5. Absorption spectra of pristine and tin substituted CeO_2 NPs.

of the sensor to humidity, the resistance changes and this behaviour was observed for all environments, such behaviour was reported before.[25] The sensitivity of the sensor was calculated based on the resistance of the sensor in air and the resistance in humid air as follows[26]:

$$S\ (\%) = \frac{100 \times (R(RH=0) - R(RH))}{R(RH=0)} \times 100 \qquad (3)$$

The sensitivity of the sensor in different environments was obtained. In an ideal environment, the test should be performed in a closed chamber under fixed parameters like humidity, pressure, temperature, etc.[27] Sensitivity of pristine CeO_2 NP sensor was 64.47% in an ideal environment. Also, sensitivity was 62.21% in a real environment. The sensitivity has showed negligible decrease in a real environment. In the real environment, humidity, temperature and pressure were varied owing to the environmental changes and the related parameters

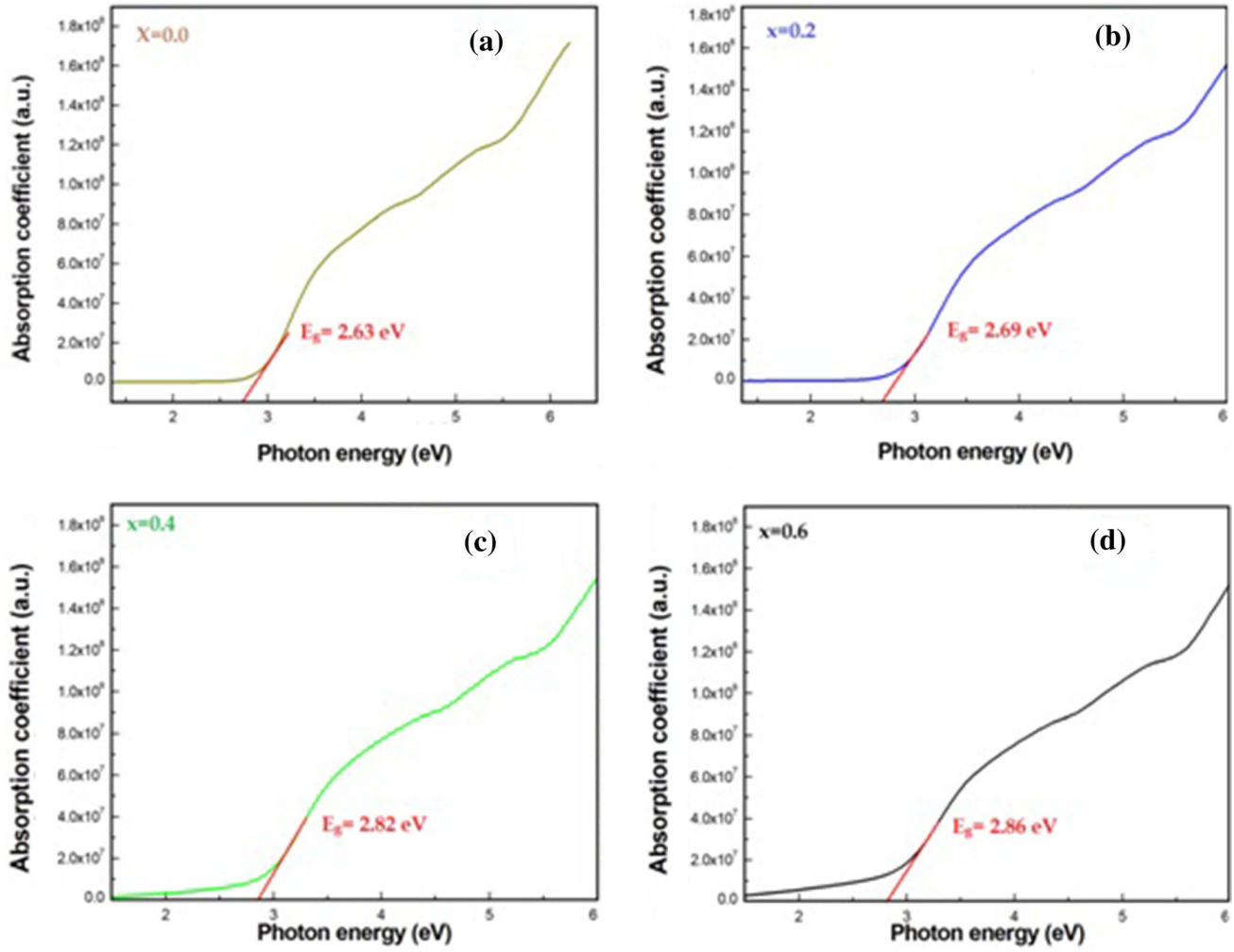

Fig. 6. (a) Band gap energy of pristine and (b–d) tin substituted CeO_2 NPs.

cannot be easily controlled. Furthermore, sensitivity was significantly reduced in a corrosive environment. Sensitivity of the sensor was 45.85% in a corrosive environment. A large number of corrosive ions are produced using saturated sodium hydroxide solution which can produce a thin oxidizing layer on the surface of the NPs. In fact, the oxidation reaction occurs between corrosive ions and CeO_2 NPs and this produces a corrosion layer on the surface of the sensing NPs. This corrosion layer decreases the sensitivity of the sensor.[25]

Figure 8a, b, c, d, e and f depicts sensing characteristics of tin substituted CeO_2 NPs (x = 0.2). In this context, due to the formation of a large number of open pores on the surface of the NPs, the sensitivity increases. The final values of the sensitivity in different environments namely, ideal, real and corrosive environments were 65.50%, 60.20% and 43.68%, respectively. Figure 9a, b, c, d, e and f provides the sensing characteristics of tin substituted CeO_2 NPs (x = 0.4). As it can be seen, the sensitivity increases due to reduction of the particle size, which provides higher surface area for the adsorption of the water molecules. The sensitivity of the sensor in three aforementioned environments was 72.66%, 68.37% and 43.98%, respectively. Figure 10a, b, c, d, e and f shows the sensing properties of the sensor with x = 0.6. For this sensor, the sensitivity values for three mentioned environments were 82.99%, 78.67% and 54.08%, respectively, which can be attributed to the ultrafine particles of this sensor.

Sensing mechanism of pristine tin substituted CeO_2 sensor is based on the Grotthuss chain reaction.[28] The adsorption of water molecule takes place on the surface of the sensor during the injection of humidity. Accordingly, a chemisorbed layer is formed between the adsorbed water molecules and metal ions from the material. As a result, the water molecules become ionized and an electric field produces formation of hydronium ions. At higher concentrations of the humidity, a continuous adsorption layer was formed which led to higher sensitivity of the sensor. In other words, a

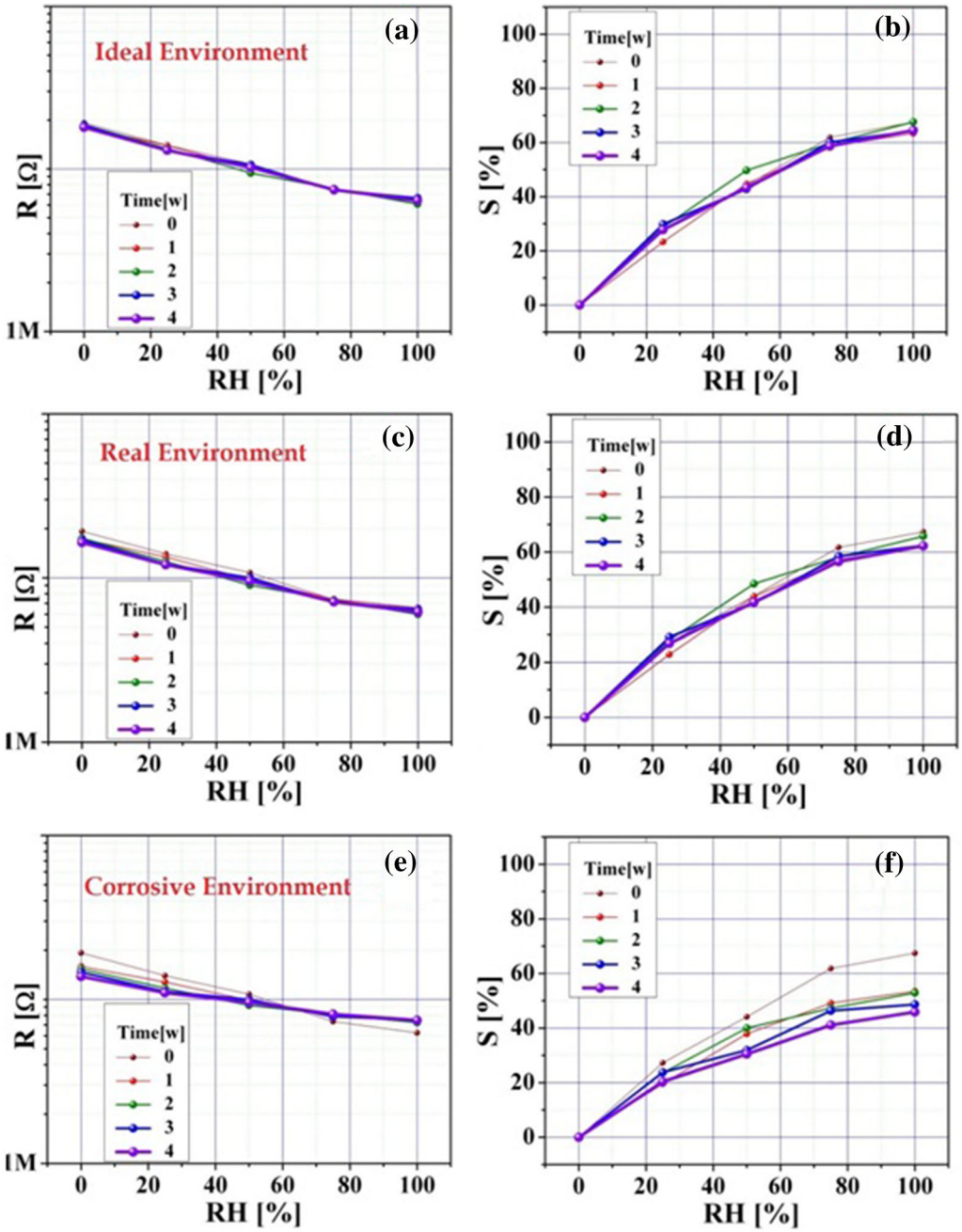

Fig. 7. Humidity sensing behaviour of pristine CeO_2 NPs at different environments.

discontinued adsorption layer is formed at lower concentrations of humidity which leads to release of a less number of hydronium ions and a low sensitivity.

Figures 7, 8, 9 and 10, show the reproducibility of pristine and tin substituted CeO_2 NP sensor in three different environments. Reproducibility test was performed after 4 weeks. Almost the same sensitivity values were found in real and ideal environments. The fabricated sensor exhibits 95% reproducible results in ideal and real environments. However, in the corrosive environment, the sensitivity was significantly decreased. Since with time, a thicker corrosive layer can be formed on the surface of NPs, accordingly, more water molecules can be trapped on this layer and consequently, less number

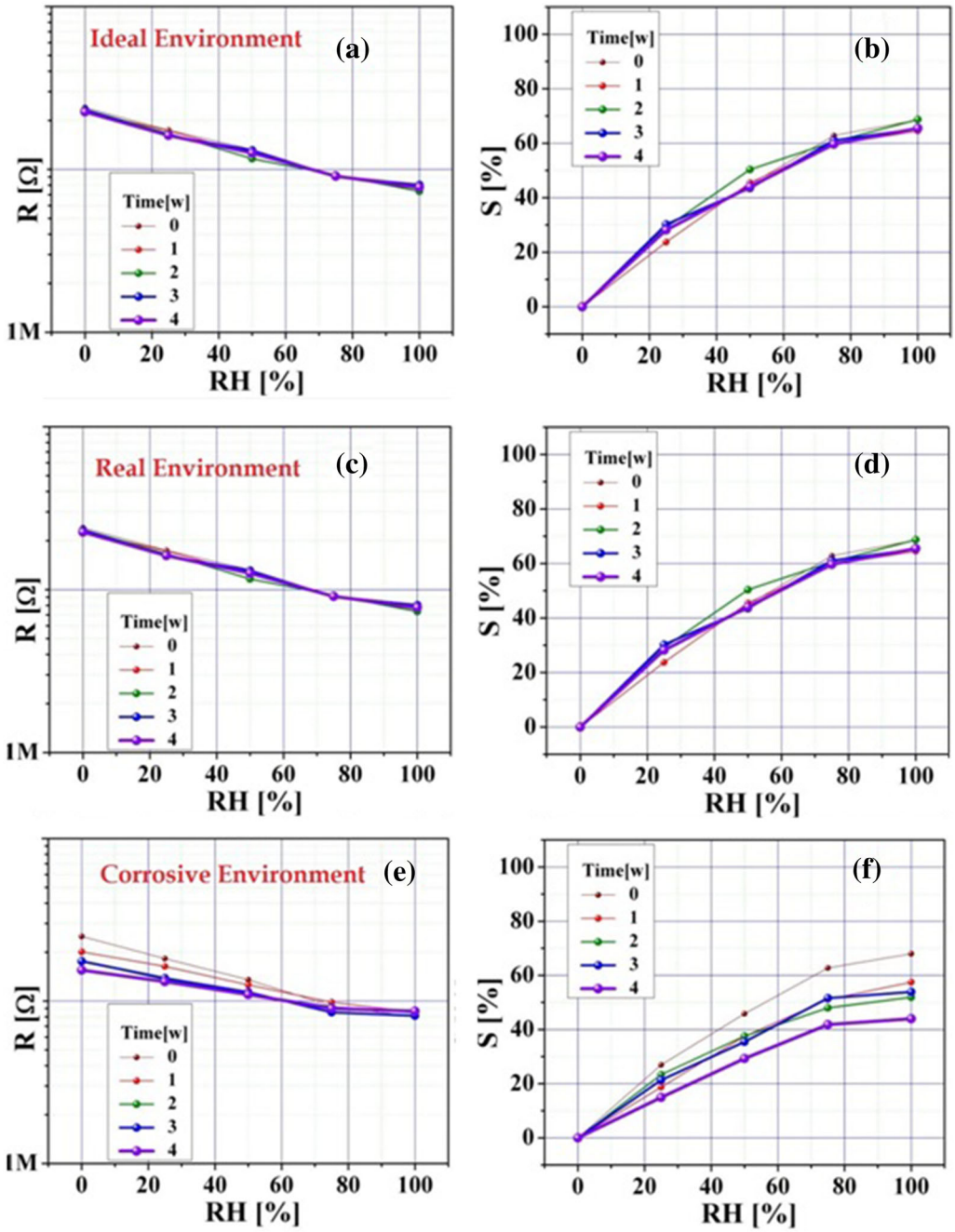

Fig. 8. Humidity sensing behaviour of $Ce_{1-x}Sn_xO_2$, NPs at different environments.

of water molecules can reach to the surface of the sensor, leading to significant decrease of sensitivity. In summary, the sensitivity of the sensor was increased with decrease of the particle size and tin content.[29] Even though the overall price of the sensor is increased by higher amounts of tin element, however, at higher tin concentrations, the sensitivity increases. For small amounts of tin, the sensors are stable in real (weak corrosive) environments and are more sensitive to humidity than a pristine CeO_2 sensor.

CONCLUSIONS

In brief, nanocrystalline pristine and tin substituted CeO_2 NPs were prepared using the microwave oven method. The results of the characterization analyses by EDAX, SEM and TEM approved the

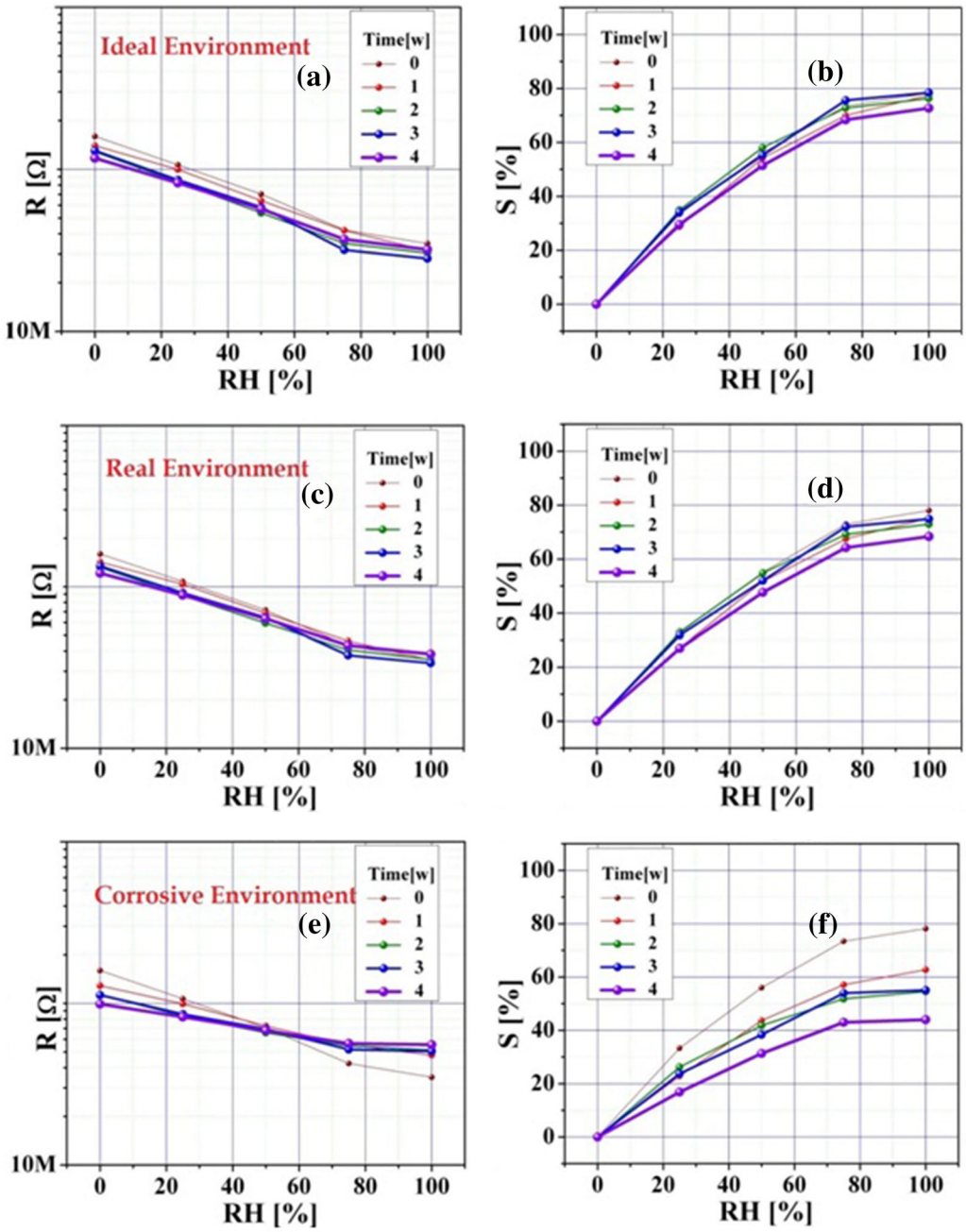

Fig. 9. Humidity sensing behaviour of $Ce_{0.6}Sn_{0.4}O_2$ NPs at different environments.

formation of NPs with desired composition and morphology. Furthermore, the Fourier-transform infrared spectrum confirmed the formation of pristine and tin substituted CeO_2 NPs. Based on the humidity sensing analysis, the prepared sensor showed a superior response in ideal and real environments and reproducibility of the sensor was 95%. Humidity sensing properties were enhanced due to the substitution of tin element. Also the tin substituted sensor showed a higher stability relative to that of a pristine sensor. Furthermore, the particle size greatly enhanced the

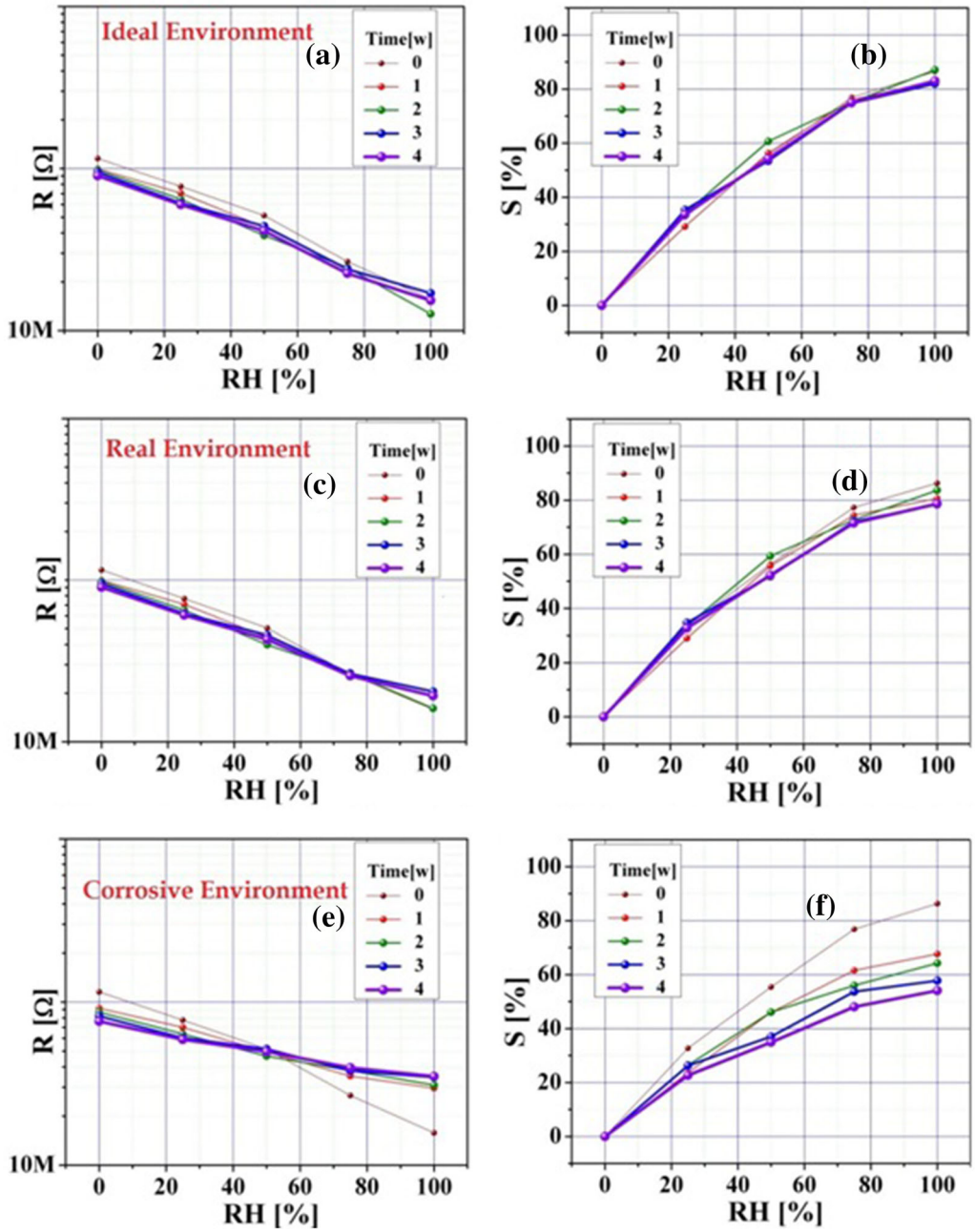

Fig. 10. Humidity sensing behaviour of $Ce_{0.4}Sn_{0.6}O_2$ NPs at different environments.

sensitivity of the sensor. Based on the results obtained in this study, tin substituted CeO_2 NPs are a promising sensing material for practical application, where the concentration of water molecules in an environment should be continuously controlled.

REFERENCES

1. A. Arumugam, C. Karthikeyan, A.S. Haja Hameed, K. Gopinath, S. Gowri, and V. Karthika, *Mater. Sci. Eng., C* 49, 408 (2015).
2. S.B. Khan, M. Faisal, M.M. Rahman, and A. Jamal, *Sci. Total Environ.* 409, 2987 (2011).
3. T.S. Sreeremya, K.M. Thulasi, A. Krishnan, and S. Ghosh, *Ind. Eng. Chem. Res.* 51, 318 (2012).
4. E.K. Goharshadi, S. Samiee, and P. Nancarrow, *J. Colloid Interface Sci.* 356, 473 (2011).
5. S. Thakur and P. Patil, *Sens. Actuators B Chem.* 194, 260 (2014).
6. Y. Lu, Z. Wang, S. Yuan, L. Shi, Y. Zhao, and W. Deng, *RSC Adv.* 3, 11707 (2013).
7. D. Bauskar, B.B. Kale, and P. Patil, *Sens. Actuators B Chem.* 161, 396 (2012).
8. X.Q. Fu, C. Wang, H.C. Yu, Y.G. Wang, and T.H. Wang, *Nanotechnology.* 18, 14 (2007).
9. V. Manikandan, X. Li, R.S. Mane, and J. Chandrasekaran, *J. Electron. Mater.* 47, 3403 (2018).

10. S.B. Bošković, D.R. Djurović, S.P. Zec, B.Z. Matović, M. Zinkevich, and F. Aldinger, *Ceram. Int.* 34, 2001 (2008).
11. C. Peng and Z. Zhang, *Ceram. Int.* 33, 1133 (2007).
12. M. Palard, J. Balencie, A. Maguer, and J.F. Hochepied, *Mater. Chem. Phys.* 120, 79 (2010).
13. V.R. Khadse, S. Thakur, K.R. Patil, and P. Patil, *Sens. Actuators B Chem.* 203, 229 (2014).
14. N. Parvatikar, S. Jain, S.V. Bhoraskar, and M.V.N. Ambika Prasad, *J. Appl. Polym. Sci.* 102, 5533 (2006).
15. A. Kumar, S. Babu, A.S. Karakoti, A. Schulte, and S. Seal, *Langmuir* 25, 10998 (2009).
16. M. Guo, J. Lu, Y. Wu, Y. Wang, and M. Luo, *Langmuir* 27, 3872 (2011).
17. B. Choudhury and A. Choudhury, *Curr. Appl. Phys.* 13, 217 (2013).
18. V.N. Morris, R.A. Farrell, A.M. Sexton, and M.A. Morris, *J. Phys: Conf. Ser.* 26, 119 (2006).
19. A.I.Y. Tok, S.W. Du, F.Y.C. Boey, and W.K. Chong, *Mater. Sci. Eng., A* 466, 223 (2007).
20. S. Phoka, P. Laokul, E. Swatsitang, V. Promarak, S. Seraphin, and S. Maensiri, *Mater. Chem. Phys.* 115, 423 (2009).
21. M. Darroudi, S.J. Hoseini, R. Kazemi Oskuee, H.A. Hosseini, L. Gholami, and S. Gerayli, *Ceram. Int.* 40, 7425 (2014).
22. V. Manikandan, A. Vanitha, E. Ranjith Kumar, and J. Chandrasekaran, *J. Magn. Magn. Mater.* 432, 477 (2017).
23. V. Manikandan, S. Sikarwar, B.C. Yadav, and R.S. Mane, *Sensors Actuators A. Phys.* 272, 267 (2018).
24. A.A. Ansari, J. Labis, M. Alam, S.M. Ramay, N. Ahmad, and A. Mahmood, *Phase Transit.* 89, 261 (2016).
25. V. Manikandan, I. Petrila, S. Vigneselvan, R. Dharmavarapu, S. Juodkazis, S. Kavita, and J. Chandrasekaran, *J. Mater. Sci.: Mater. Electron.* 29, 18660 (2018).
26. I. Petrila, K. Popa, and F. Tudorache, *Sens. Actuators A Phys.* 247, 156 (2016).
27. S. Sikarwar, B.C. Yadav, S. Singh, G.I. Dzhardimalieva, S.I. Pomogailo, N.D. Golubeva, and A.D. Pomogailo, *Sens. Actuators B Chem.* 232, 283 (2016).
28. S. Sikarwar and B.C. Yadav, *Sens. Actuators A Phys.* 233, 54 (2015).
29. B.C. Yadav, S. Sikarwar, A. Bhaduri, and P. Kumar, *Int. Adv. Res. J. Sci. Eng. Technol.* 2, 105 (2015). https://doi.org/10.17148/IARJSET.2015.21122.
30. T. Thiwawong, K. Onlaor, and B. Tunhoo, *Adv. Mater. Sci. Eng.* 2013, 640428 (2013). https://doi.org/10.1155/2013/640428.
31. N.D. Md Sin, S. Ahmad, M.F. Malek, M.H. Mamat, and M. Rusop, *IOP Conf. Ser.: Mater. Sci. Eng.* 46, 012005 (2013).
32. M. Ghadiry, M. Gholami, C.K. Lai, H. Ahmad, and W.Y. Chong, *PLoS ONE* 11, e0153949 (2016).
33. Karunesh Tiwari, *Res. J. Nanosci. Nanotechnol.* 7, 10 (2017).
34. A. Panwar, N.K. Pandey, and S.K. Misra, *IJESRT* 7, 179 (2018).
35. Pranlekha Traiwatcharanon, Kriengkri Timsorn, and Chatchawal Wongchoosuk, *Mater. Res. Express* 4, 085038 (2017).